Ceramics International 50 (2024) 188–196

Contents lists available at ScienceDirect

Ceramics International

journal homepage: www.elsevier.com/locate/ceramint

Microstructure and mechanical properties of an experimental lithium disilicate dental glass-ceramic

Bruna de F. Vallerini [a], Laís D. Silva [b], Mariana de O.C. Villas-Bôas [b], Oscar Peitl [b], Edgar D. Zanotto [b], Lígia A.P. Pinelli [a,*]

[a] Department of Dental Materials and Prosthodontics (FOAr/Unesp), Araraquara, SP, 14801-903, Brazil
[b] Center of Research, Technology, and Education in Vitreous Materials (CeRTEV), Department of Materials Engineering (DEMa), Federal University of São Carlos (UFSCar), 13565-905, São Carlos, SP, Brazil

ARTICLE INFO

Handling Editor: Dr P. Vincenzini

Keywords:
Glass-ceramics
Dental materials
Mechanical properties

ABSTRACT

After testing over 50 experimental lithium disilicate (LS2)-based glass-ceramic (GC) compositions and evaluating their glass-forming ability and the effect of various heat treatments on their crystallized fraction, crystal size, and morphology, a particularly promising formulation was selected for the optimization of the mechanical properties of materials. The specimens were divided into groups submitted to a nucleation heat treatment at different times and temperatures, i.e., T1 (500 °C/90′), T2 (500 °C/180′), T3 (500 °C/360′) and T4 (480 °C/360′), followed by a crystal growth treatment to induce the lithium metasilicate (700 °C) and LS2 (840 °C) phases. However, a third (minor) phase, lithium phosphate, also precipitated. IPS e.max CAD was used as the control group (C, 500 °C/360′). The elastic modulus (E) was measured by the impulse excitation technique (ASTM E 1876-15), while the Vickers hardness (HV) and biaxial flexural strength (BFS) were determined by indentation and the piston-on-three balls test (ISO 6872), respectively. The E and HV results were analyzed by ANOVA one-way with Games–Howell post-hoc test, whereas the BFS data were investigated by Kruskal-Wallis with Dunn's post-hoc test ($\alpha = 0.05$). The E of all GCs were within the expected range for commercial LS2 glass-ceramics. The T2 and T4 GCs exhibited the best properties when compared to the C group, and despite their relatively small crystallized fraction (~57 %), they showed a hardness of 5.8 ± 0.2 GPa, a value that is adequate and statistically equal to that of the control group. The same groups reached BFS values of 359 ± 89 MPa and 493 ± 147 MPa, respectively, which are also statistically equal to that of the C group (338 ± 61 MPa). The mechanical properties of the material studied was successfully optimized through variations in the nucleation temperature and time, reaching values comparable to (but not better than) commercial dental glass-ceramics.

1. Introduction

Glass-ceramics (GCs) are inorganic, non-metallic materials prepared by the controlled crystallization of glasses via different processing methods. They contain at least one type of functional crystalline phase and residual glass, reaching a crystallized volume fraction that may vary from ppm to almost 100 % [1]. Glass-ceramics have been the material of choice for aesthetic restorations, especially anterior teeth, due to their ability to mimic dental tissues, biocompatibility, chemical durability in the buccal environment, and adequate mechanical properties [2–6].

Lithium disilicate-based glass-ceramics ($Li_2O{\cdot}2SiO_2$) are one of the most successful commercial materials in dentistry [7], being widely chosen by many professionals because of their wide range of application in veneers, crowns, and fixed dental prostheses with up to three-units. These GCs exhibit a high flexural strength of 300–400 MPa, a high fracture toughness of 2.8–3.5 MPa $m^{½}$, a hardness similar to that of natural teeth, high chemical durability, translucency, and attractive aesthetics [8–10]. The possibility of being easily milled (in a partially crystallized state containing lithium metasilicate crystals) is also crucial, as it simplifies the prosthesis manufacturing methods and allows their production in laboratories and chairside systems through computer-aided design/computer-aided manufacturing (CAD/CAM) technology, resulting in worldwide clinical approval [11,12]. Despite these positive combinations of properties, the strength of these glass-ceramics is not yet sufficient to produce dental prostheses with a greater number of elements, as well as fixed implant-supported

* Corresponding author. 1680 Humaitá Street, Araraquara, SP, 14801-903, Brazil.
E-mail address: ligia.pinelli@unesp.br (L.A.P. Pinelli).

https://doi.org/10.1016/j.ceramint.2023.10.093
Received 2 August 2023; Received in revised form 29 September 2023; Accepted 10 October 2023
Available online 11 October 2023

prostheses, such as those produced with yttria-stabilized tetragonal zirconia polycrystal (Y-TZP) [13–17].

The properties of GCs depend on their chemical composition and the heat treatment adopted, which in turn impact their microstructural characteristics, e.g., crystal type, size and morphology, and crystallized fraction [1,7,18,19]. The conventional route for glass-ceramic production involves the development of a base glass, which is melted and vitrified, followed by a double heat treatment: one for internal nucleation, normally around the glass transition temperature (T_g), and another to foster crystal growth, which significantly affects the phases formed, the crystal size distribution and the crystallized volume fraction [1]. These microstructural characteristics are therefore controlled through parent glass composition, nucleation, and crystal growth treatments [18,20–22], which strongly influence the mechanical [10,23,24], chemical and optical [6,25,26] properties of GCs.

Over the years, a vast literature have shown that glass-ceramics are being used in many fields due to their unique combination of positive features, attracting the interest of academic scientists and industrial researchers, especially in dentistry [18]. The focus of many researches is to understand glass-ceramics in order to further improve their properties [1,3,7,18,21,27–30]. For example, Riquieri et al. [27] observed important effects of crystallized fraction on the flexural strength of GCs. Albakry et al. [31] and Serbena et al. [7] also analyzed the importance of crystallized fraction and concluded that it directly impacts the mechanical properties of materials by increasing their elastic modulus and producing crack bowing and deflection at crystalline grains/residual glass interfaces [7,31,32]. This effect is largely associated with the lath-shaped morphology of LS2 crystals. During crack bowing or deflection, the crack path increases and more energy is consumed to improve the material toughness [7,18,25,33].

In the intermediate stages of crystallization, when lithium metasilicate crystals precipitate, LS2-based glass-ceramics can be easily machined into desired shapes. Afterwards, an additional heat treatment forms lithium disilicate crystals, which in turn further increases their fracture strength and toughness [7]. This microstructure is characterized by a high crystallinity ranging from 50 % to 80 %, and a high aspect ratio of the grains, which impairs crack propagation [7,10,25,28,29,33–40].

It is usually hypothesized that the greater the translucency and aesthetics of these glass-ceramics, the lower their fracture strength because of the larger fraction of residual glass. In the case of LS2 glass-ceramics, the microstructure is typically composed of one or more crystalline phases embedded in a glassy matrix [7], resulting in a high crystallinity, with the lath-like lithium disilicate crystals ranging from 1 to 10 μm [7,18]. In addition to lithium disilicate ($Li_2Si_2O_5$), other crystal phases are normally present, for instance, lithium metasilicate (Li_2SiO_3), lithium phosphate (Li_3PO_4), and α-quartz (SiO_2) [41]. This configuration of interlocked lath-shaped or plate-like crystals is responsible for their superior mechanical strength [7,28].

Even though there are hundreds of papers and patents on LS2-LS glass-ceramics, a crucial question still remains: **Is it still possible to further optimize their properties**?

After testing over 50 new, experimental lithium disilicate (LS2) glass-ceramic compositions over the past 6 years [30] and evaluating the effect of various heat treatments on the crystallized fraction, crystal size and morphology of these materials, as well as on their resulting mechanical properties as reported in our previous work [30], for this study **we selected a particularly promising composition** intended for CAD/CAM, which in preliminary tests showed properties similar to those of successful commercial glass-ceramics. During a particular heat treatment, it was possible to observe a microstructure of lath-shaped interlocked crystals smaller than 3.5 μm. Furthermore, the lithium metasilicate and disilicate phases exhibited distinct plate-like and lath-shaped morphologies, respectively, and were easily identified after their respective crystal growth heat treatments [30]. Thus, it can be inferred that this experimental glass-ceramic material has potential for further exploration and optimization.

Therefore, this study focused on the evaluation of the above-described lithium disilicate (LS2)- and lithium metasilicate (LS)-based glass-ceramic composition named LSM CAD developed at the Laboratory of Vitreous Materials (LaMaV) of the Federal University of São Carlos (UFSCar). In the case of this specific lithium disilicate developed, the primary purpose was to expand the range of applications for lithium disilicate material, ultimately aiming to create a final product capable of producing larger prosthetic components, characteristics do not present in the commercial one. Thus, continually aiming to advance materials with a particular focus on improving their microstructural characteristics in order to improve their mechanical properties. The aim was to investigate if its mechanical properties could be further improved in relation to those of the (already) excellent commercial glass-ceramics. For this purpose, different nucleation times and temperatures were used, always keeping the crystal growth treatment constant to promote microstructural changes. Then, crystal phase and microstructure analyses, along with elastic modulus, Vickers hardness, and biaxial flexural strength measurements, were performed. Ivoclar's IPS e.max CAD was adopted as a reference material.

The study in question presents two defined null hypotheses (H_0) as follows: H_{01} - There is no difference in the microstructural characteristics between the commercial material IPS e.max CAD (Ivoclar Vivadent) and the experimental materials; H_{02} - There is no difference in the mechanical properties between the commercial material IPS e.max CAD (Ivoclar Vivadent) and the experimental materials.

2. Materials and methods

The material designated for analysis was the experimental CAD/CAM material lithium disilicate-based glass (LSM CAD), which has the following composition: 50–60 % SiO_2, 20–30 % Li_2O, 0–10 % K_2O, 0–10 % P_2O_5, 0–5% CaO, 0–5% BaO, 0–5% Al_2O_3, 0–5% MgO, 0–5% Sb_2O_3. To prepare this selected material, the following analytical grade chemicals were used: aluminum oxide (Alfa Aesar, 99.9 %), antimony oxide III (Vetec, 99.5 %), barium carbonate (Qhemis, 99.0 %), calcium carbonate (J.T. Baker, 99.3 %), lithium carbonate (Synth,99.0 %), magnesium oxide (Synth, 96 %), monobasic potassium phosphate (Vetec, 99.0 %), potassium carbonate (Sigma-Aldrich, 99.0 %), silicon dioxide (Vitrovita quartz #4, 99.99 %). The mixture of reagents was homogenized in a Turbula® (Wab Group, Muttenz, Switzerland) for 4 h and then melted in a platinum crucible placed in an electric furnace at 1450 °C for 3 h. The melt was quenched in air onto a steel plate and re-melted three times to eliminate bubbles and streaks and homogenize the viscous liquid. Finally, it was cast in a stainless-steel cylindrical mold (12 mm in diameter x 35 mm in length).

The annealing procedure of the glass samples was carried out in an EDG 7000 (EDG, São Carlos, São Paulo, Brazil) furnace at 380 °C (53 °C below T_g = 433 °C) for 2 h to relieve residual thermal stresses. The specimens were cut using an SYJ-150 Low-Speed Diamond Saw (MTI, Richmond, California, USA) with a diamond blade (Series 15LC Diamond, Buehler, Illinois, USA) at 200 rpm and water-cooled.

The cylindrical glass samples obtained were cut into discs of 12 mm in diameter x 1.2 mm in thickness following the ISO 6872 [42] for flexural strength measurements, that is biaxial flexural strength (by the piston-on-three balls test, n = 10 per group). In addition, the same dimension of samples were used to determine the crystalline fraction (n = 3 images per group), crystal size distribution (n = 3 images per group), elastic modulus (n = 4 per group, 4 measurement in one sample) and Vickers hardness (n = 6 per group, 3 measurement in one sample). The sample dimensions were measured using a digital caliper (500-144B, Mitutoyo Sul Americana, Suzano, SP, Brazil), accepting a variation of ±0.01 mm. Each value represents the average of three measurements.

The samples were randomly divided and submitted to three crystallization steps, namely, nucleation, lithium metasilicate (LS) growth, and LS2 growth. The time and temperature of the nucleation heat treatment were varied to obtain different microstructures in an attempt

to optimize the mechanical properties of the glass-ceramics, forming four groups: T1, T2, T3, and T4, as shown in Table 1.

After the heat treatments, the samples were ground using silicon carbide (SiC) abrasive papers of different granulometry (from 150 to 1200 grit) followed by polishing on an aqueous suspension with 1 μm cerium oxide (CeO2).

Ivoclar's IPS e.max CAD was used as the control group (C group), and the blocks were machined into a cylindrical shape. The cylinders were cut in the same dimension for all the experimental groups to yield discs with 12 mm in diameter x 1.2 mm in thickness. The crystallization cycle was carried out in a Programat P310 furnace (Ivoclar Vivadent, Schaan, Liechtenstein), according to the manufacturer's recommendations. The finishing and polishing of the IPS e.max CAD specimens followed the same procedures described for the LSM groups.

All groups were analyzed on an X-ray diffractometer (XRD) (RINT-2000, RIGAKU, Tokyo, Japan) with Cu-Kα radiation in a scan range between 10° and 80° at 3°/min. The crystalline phases were identified with the aid of the JCPDS-ICDD database [43,44]. The crystallized volume fraction (CF - %) was obtained from the ratio of the crystalline area (A_C) to the total area (A_T) of the diffractograms using Equation (1) below [33,45,46]:

$$CF = (A_C / A_T) \text{ x } 100 \quad (1)$$

The crystal size distributions, morphologies, and crystallized fractions of the heat-treated samples were measured using the images obtained on a scanning electron microscope (SEM Jeol, JSM6610LV, Akishima, Tokyo, Japan). The samples were cleaned by ultrasound and covered with a thin layer of Au–Pd. Three images from each group were selected. Standardization of contrast and brightness was performed using Fotor Photo Editor (version 3.5.1), excluding image borders and information bars. The crystal sizes and crystallized fractions were measured with the aid of Image J software (National Institutes of Health, Bethesda, Maryland, USA) [47,48] with the Make Binary function, which converts the images to black and white, allowing a more accurate estimate of the desired features.

The elastic modulus (E) was determined using the impulse excitation technique (Sonelastic, ATCP, Brazil) following ASTM E 1876-15 standard [49]. The dynamic elastic modulus is calculated by Sonelastic Software using equations provided by the ASTM standard, which considers the geometry, mass, sample dimensions, and frequencies obtained through the equipment [49,50]. The results were obtained from four specimens of each group, with an average of four measurements per specimen.

Microhardness was evaluated by the Vickers indentation (HV) technique with the aid of a microhardness tester (Future-Tech F-7e, Tokyo, Japan) with a Vickers-type diamond indenter, according to ASTM C 1327-03 [51]. The experiments were carried out by applying 500 gf at a loading time of 15 s at room temperature (20 °C, 52 % of air humidity). A distance of at least 0.5 mm between the indentations was considered to avoid interference from the residual stress fields of the previous indentations. For statistics, at least six indentations were performed in each sample.

Biaxial flexural strength (BFS) was measured by the piston-on-three balls test at room temperature (24 °C, 56 % of air humidity) on a universal testing machine (EMIC DL 200 Equipment and Systems Testing Ltd.). Each specimen was centrally placed over three spheres (with a diameter of 2.5 mm, positioned 120° apart on a support circle with a diameter of 12 mm) and loaded by the piston in the center of the opposite surface, following ISO 6872 standard [42]. A 0.5 mm/min displacement rate was adopted, and 10 samples were tested for each glass-ceramic.

The biaxial bending strength (BFS) of the materials was evaluated using Equations (2)–(4), as proposed by Ref. [42]:

$$S = \frac{-0.2387\ P\ (X - Y)}{d^2}, \quad (2)$$

where S is the biaxial flexural strength (MPa), P is the total load causing fracture (N), and d is the specimen thickness at the fracture origin (mm). X and Y were determined according to Equations (3) and (4) [42]:

$$X = (1+\nu) ln \left(\frac{r_2}{r_3}\right)^2 + \frac{(1-\nu)}{2}\left(\frac{r_2}{r_3}\right)^2, \quad (3)$$

$$Y = (1+\nu)\left[(1+ln)\left(\frac{r_1}{r_3}\right)^2\right] + (1-\nu)\left(\frac{r_1}{r_3}\right)^2, \quad (4)$$

where ν is the Poisson's ratio (the value assumed for the present study was 0.25), r_1 is the radius of the support circle, r_2 is the radius of the loaded area, r_3 is the radius of the specimen, and d is the specimen thickness at the fracture origin.

The E and HV data were statistically analyzed using ANOVA one-way with Games–Howell post-hoc ($\alpha = 0.05$), while the BFS and CSD results were statistically analyzed by Kruskal-Wallis with Dunn's post-hoc test ($\alpha = 0.05$), and the CF data were analyzed by descriptive statistics.

Table 1
Time and temperature of nucleation, lithium metasilicate and lithium disilicate growth treatments applied to the four experimental groups.

Group	Time (min)	Temperature (°C)	LS Crystal Growth (°C)	LS2 Crystal Growth (°C)
T1	90	500	700	840
T2	180	500	700	840
T3	360	500	700	840
T4	360	480	700	840

3. Results

A visually homogeneous transparent glass was obtained after melting and annealing. The glass was named LSM CAD. It is composed of 50–60 % SiO_2, 20–30 % Li_2O, 0–10 % K_2O, 0–10 % P_2O_5, 0–5% CaO, 0–5% BaO, 0–5% Al_2O_3, 0–5% MgO, 0–5% Sb_2O_3, a composition similar to that of the control group (IPS e.max CAD), which is 57–80 % SiO_2, 11–19 % Li_2O, 0–13 % K_2O, 0–11 % P_2O_5, 0–8% ZrO_2–ZnO,0–5% Al_2O_3, 0–5% MgO, and coloring oxides.

Four different nucleation heat treatments were carried out, namely, T1 (500 °C–90 min), T2 (500 °C–180 min), T3 (500 °C–360 min), and T4 (480 °C–360 min), as described in Table 1. SEM micrographs were obtained after each heat treatment (Fig. 1).

The micrographs in Fig. 1 show a fine microstructure of lath-shaped crystals embedded in a glassy matrix with uniform dimensions, in addition to an interlocking pattern of crystals that resemble the control group (Fig. 1 e – IPS e.max CAD). However, the images of T2 and T3 (Fig. 1 b and c, respectively) reveal two distinct crystal sizes.

The XRD patterns of each heat treatment are shown in Fig. 2. All crystalline phases were identified.

From Fig. 2., it is possible to observe that the specimens of groups T1, T2, T3, and T4 showed a predominance of lithium disilicate crystals – $Li_2Si_2O_5$ (ICDD Card. no.82-2396), in addition to the presence of lithium phosphate – Li_3PO_4 (ICDD Card. no.83-339) and lithium metasilicate crystals – Li_2SiO_3 (ICDD Card. no.70-330). The results are similar to that of the control group, except for that fact the latter does not have lithium metasilicate in its composition.

The crystallized volume fractions were estimated from the ratio of the crystalline area to the total area of the diffractograms [33,45,46]. Table 2 shows the resulting phase percentages.

The X-ray diffraction analysis indicated that all experimental groups had a slight variation in the phase quantities, with values ranging between 47 and 50 % for lithium disilicate, 4–5% for lithium phosphate, and 3–4% for lithium metasilicate (Table 2). The control group, in contrast, showed a predominance of lithium disilicate (59 %), with the

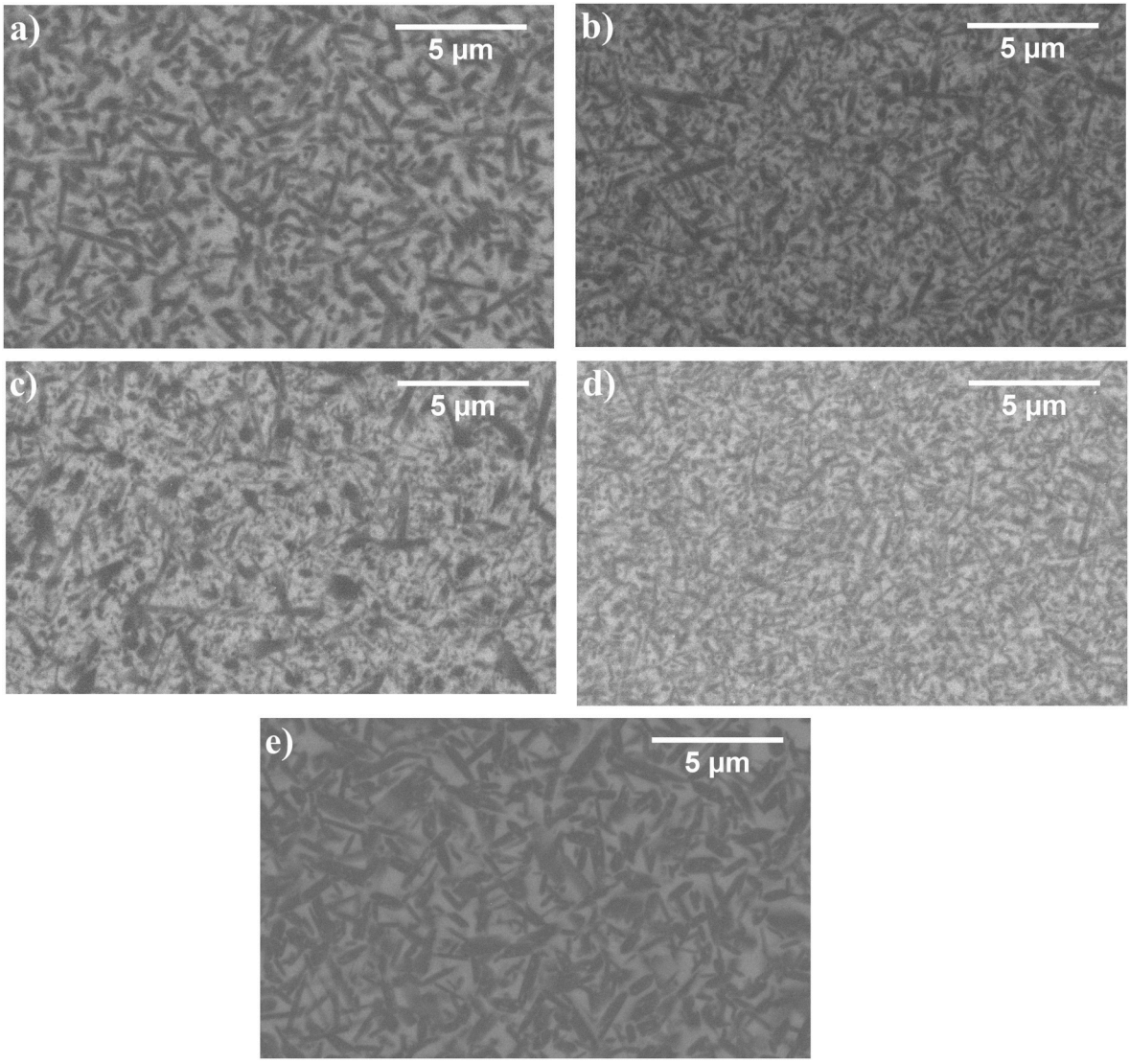

Fig. 1. SEM micrographs of a) T1 (500 °C–90 min), b) T2 (500 °C–180 min), c) T3 (500 °C–360 min), d) T4 (480 °C–360 min) and e) IPS e.max CAD glass-ceramics.

presence of lithium phosphate (6 %) and the absence of lithium metasilicate, corroborating the values obtained by Lubauer et al. [52] (~63 and 7 %, respectively). It is worth mentioning that in this work the crystallized fraction was calculated by the peak area method (Equation (1)).

Regarding the crystallized fraction and residual glass phase, from Table 2 it is possible to observe a **small** crystallized fraction for the experimental groups (T1, T2, T3 and T4) in comparison with the control sample. Considering constant crystal growth temperatures and times, as the nucleation time (Table 1) increased from 90 to 180 min at 500 °C for samples T1 and T2, respectively, the crystallized fraction slightly increased from 54 to 58 %.

As for groups T3 and T4, even with the decrease in the nucleation temperature from 500 to 480 °C, respectively, the crystallized fraction remained practically constant (57 %), indicating that there was a saturation of the number of nuclei at 480 °C for 360 min, which did not affect the total crystallized fraction. Despite this small crystallized fraction of our samples compared to the control group and the consequent increase in the residual glass phase, this microstructure is still promising due to its reasonably high crystallized volumetric fraction (54%–58 %), a parameter that strongly affects the flexural strength of materials, as reported by Peitl et al. [53] and Serbena et al. [7].

Table 3 summarizes the means of crystal size distribution (CSD), elastic modulus (E), Vickers hardness (HV), and biaxial flexural strength (BFS) obtained for T1, T2, T3 and T4 in comparison with the control group (IPS e.max CAD).

As observed in Table 3, the crystal size distributions of groups T1 and T2 were approximately 2 μm and did not differ statistically from those of the control group, unlike T3 and T4, which exhibited larger and smaller crystal sizes (3.1 μm and 1.6 μm), respectively. The elastic modulus of T1 and T4 did not differ statistically, reaching a value of ~95 GPa. Only the E of T3 was statistically equal to that of the control group, with a value of ~100 GPa. With respect to Vickers hardness, only groups T2 and T4 presented a value (~5.8 GPa) comparable to the control (6 GPa), yet not statistically different. In contrast, groups T1 and T3 showed lower and significantly different values (5.6 and 5.5 GPa, respectively).

Despite the differences between the crystallized fractions of the control group and the GCs studied herein, they were not enough to significantly affect the results of biaxial bending strength, since T1, T2, and T4 did not differ statistically. Among all groups tested, T4 showed the best strength (493 ± 147 MPa) (Table 3), while the lowest value was achieved by T3 (225 ± 52 MPa). This lowest value may be explained by the different crystal morphology present in the microstructure and the relatively large variability in the crystal sizes, as observed in Fig. 1 c. and Table 3.

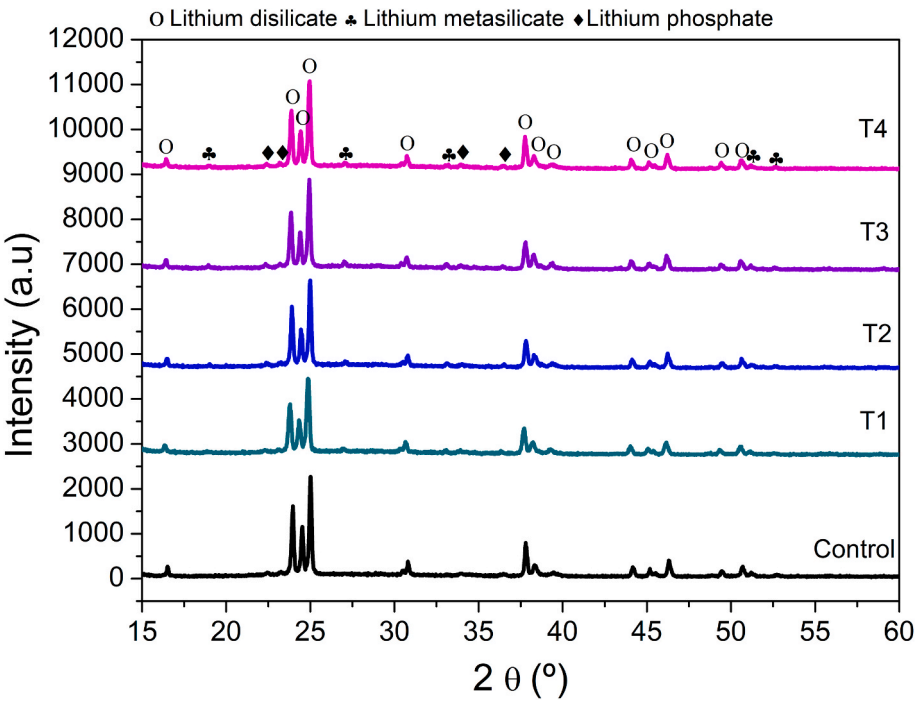

Fig. 2. X-ray diffractograms of T1 (500 °C–90 min), T2 (500 °C–180 min), T3 (500 °C–360 min), T4 (480 °C–360 min) and IPS e.max CAD (control) glass-ceramics.

Table 2
Quantitative analysis of lithium disilicate (LD), lithium phosphate (LP), lithium metasilicate (LM), overall crystallized fraction (CF), and residual glass phase (RG) present in the specimens.

Group	LD (%)	LP (%)	LM (%)	CCF (%)	RRG (%)
Control	59	6	–	65	35
T1	47	4	3	54	46
T2	50	5	3	58	42
T3	49	4	4	57	43
T4	49	5	3	57	43

Table 3
Means of crystal size distribution (CSD, in μm), elastic modulus (E), Vickers hardness, and biaxial flexural strength (BFS) of the studied glass-ceramic groups.

GROUP	CSD (μm)	E (GPa)	HV (GPa)	BFS (MPa)
Control	2.2 (0.4)^{a}	101 (2)^{a}	6.0 (0.1)^{a}	338 (61)^{a}
T1	2.1 (0.5)^{a}	95 (7)^{bc}	5.6 (0.2)^{bc}	400 (94)^{a}
T2	2.0 (0.6)^{a}	92 (9)^{b}	5.8 (0.2)^{ab}	359 (89)^{a}
T3	3.1 (0.6)^{b}	99 (1)^{ac}	5.5 (0.2)^{c}	225 (52)^{b}
T4	1.6 (0.4)^{c}	97 (4)^{bc}	5.8 (0.1)^{ab}	493 (147)^{a}

* Lowercase superscript letters indicate a statistically significant difference between rows ($p < 0.05$).

4. Discussion

The properties of glass-ceramics depend on their composition and the thermal treatments to which they are submitted [19,22]. As already reported, these thermal treatments have a significant effect on the crystallization process of GCs [22], controlling their phase formation, crystallinity, and crystal size [6]. As a result, they have been widely used to optimize the type and content of phases as well as the overall microstructure of crystals for the development of materials with desired properties [54,55].

Studies on multicomponent bioactive silicate glasses have revealed that when network-modifying ions are introduced, they cause a decrease in the glass transition temperature, along with an increase in the crystallization temperature. This effectively expands the processing window of the material under investigation [56,57]. Due to their excellent properties, such as good chemical stability, biocompatibility, translucency, and mechanical strength, these glass-ceramics have been widely used, for instance, in commercial dental restorations [58]. Dental materials with a restorative function must, therefore, demonstrate durability in the oral environment, resemble the natural structure of the tooth, and exhibit high mechanical strength and wear resistance [9].

Therefore, the addition of Al_2O_3 and ZrO_2 enhances the chemical stability of the glass, which is of great importance for dental materials [59,60],as Zr^{4+} promotes a more polymerized silicate network [61]. Meanwhile, CaO and K_2O reduce the melting temperature. In addition to lowering the melting temperature, K_2O favors the preferential nucleation of the metasilicate phase instead of the disilicate phase, as this reagent hinders the diffusion of Li_2O into the SiO_2-rich region [60], a crucial crystalline phase in the initial stage of crystallization (commonly used in commercial glass-ceramics) for the material machining step [62]. Utilizing efficient processing and manufacturing techniques can lead to dental restorative materials that boast a cost-effective production, exceptional aesthetics, and sustained mechanical and chemical performance over the long term following implantation [63].

The findings related to the XRD patterns (Fig. 2) of the LSM CAD groups comply with those reported in the literature for commercial GCs [5,7,29,64–66],which show a predominance of lithium disilicate. Huang et al. [66] and Lien et al. [29] observed that when glass-ceramics of this family are subjected to an additional crystallization treatment at temperatures above 780 °C, there is an increase in the transformation of lithium metasilicate into lithium disilicate, leading to an improvement in their mechanical properties [29,66]. Herein, both the commercial material and the LSM CAD were submitted to a heat treatment above 780 °C, that is, 820 °C for 7 min and 840 °C for 10 min, respectively. However, in the experimental materials the extra heat treatment adopted (840 °C/10 min) was not enough to transform all the lithium metasilicate into lithium disilicate, as seen by the residual lithium metasilicate (3–4%) shown in Table 2.

Thus, according to Fig. 2 and Table 2 the control group showed a predominance of lithium disilicate (59 %), with the presence of lithium phosphate (6 %) and the absence of lithium metasilicate, totaling 65 %

of crystallized volume fraction, in agreement with Belli et al. [67], who reported a crystallinity of 67–70 %. In our work, it was possible to observe that variations in the heat treatments did not cause major changes in the present phases, since all studied experimental groups exhibited an extra minority phase of lithium metasilicate (3–4%).

The analyzed phase contents varied little among the four groups (T1, T2, T3, and T4), although a small increase was noted when the nucleation time was doubled from 90 to 180 min at 500 °C, going from 54 to 58 % for T1 and T2, respectively. Nonetheless, when the nucleation time was increased to 360 min at the same temperature or 480 °C, the total crystallized fraction remained the same for T3 and T4 (~57 %), indicating a saturation of the number of nucleation sites. In their study on stoichiometric lithium disilicate, Serbena et al. [7] described an increase in the crystallized fraction as a function of nucleation treatment time and temperature [7]. Such finding does not corroborate our results, which demonstrated that variations in the nucleation time and temperature did not affect the crystallized fraction for groups T2, T3 and T4.

The nucleation heat treatments had a stronger influence on the morphology than on the crystallized fraction, since shorter nucleation times may have taken longer to saturate and the increase in time was not enough to considerably change the crystallized fraction. However, as we are dealing with a non-stoichiometric composition.

In this way, considering the focus of this research is on the study of dental glass-ceramics based on the lithium disilicate system and, therefore, on commercially applicable compositions [58], the studied composition, have a SiO_2/Li_2O molar ratio of 2.45, that deviates from the stoichiometric ratio ($SiO_2/Li_2O > 2$). The crystallization of non-stoichiometric glasses (i.e., those with that the glass composition is different from those of the precipitating crystalline phases) is a fairly common phenomenon in glass-ceramic technology [68], and of considerable practical interest (i.e., Soares et al. [69], Lubauer et al. [70], Daguano et al. [62], Villas-Boas et al. [30]). In general, the various crystalline phases that can precipitate will exhibit considerably different nucleation and growth rates.

Thus, the formation of such phases results in local and, eventually, global modifications in the composition of the remaining liquid in advanced stages of the phase transformation, when the volumetric fraction of the crystalline phases has reached a sufficiently significant size [68]. In this way, the number of nuclei may have saturated, i.e., reached a limit, owing to the depletion of nucleating agents; this may have significantly affected the crystalline fraction, as the temperatures and crystal growth times were held constant, making the crystallized fraction strongly dependent on the number of nuclei.

From the micrographs in Fig. 1, it can be seen that the crystal morphology found in all groups consists of lath-shaped crystals [9,23,25,26] and an interlocked microstructure, which is an important feature that influences the material mechanical performance [7,25,29,33,71]. The microstructure of T1 (CSD = 2.1 ± 0.5 μm) exhibited characteristics that resemble the control group (CSD = 2.2 ± 0.4 μm), resulting in a biaxial flexural strength that did not statistically differ despite the low crystallized fraction (54 %) compared to the control group (65 %). Likewise, T4 achieved statistically comparable values, that is an average crystal size of 1.6 ± 0.4 μm and a crystallized fraction of 57 %.

Samples T2 and T3 showed a wide crystal size distribution, as observed in the histogram (Fig. 3) obtained from various crystals in the micrographs (Fig. 1). Hallmann et al. [6] and Höland and Beall [63] demonstrated that differences in the mechanical properties of materials with similar chemical compositions are related to divergent microstructures. Thus, the greater crystal size distribution, length and morphology of T3 explains why this group showed a lower flexural strength (BFS = 225 ± 52 MPa and CSD = 3.1 ± 0.6 μm) despite having the same crystallized fraction as T2 and T4.

As observed, groups T1, T2 and T4 exhibited an interlocked microstructure due to a crystallized fraction >50 %, in addition to elongated shape lithium disilicate crystals homogeneously embedded in a glassy matrix, with a crystal length of 0.5–3 μm. This highly uniform crystal size associated with the needle-like morphology and high crystallized fraction can hinder crack propagation, forming an interlocked microstructure and leading to the appearance of crystals similar to those found in natural bones, as described in the literature [6,10,19,25].

As it can be seen in Fig. 4, the high crystallized fraction of T2 and T4 (58 and 57 %, respectively) in relation to T1 (54 %) increased the Vickers hardness, making these samples statistically comparable to the control group (IPS e.max CAD). In the case of T3, it followed the same trend as that observed by Peitl et al. [53], who verified that the flexural strength of samples with the same crystalline volume percentage tends to cause an increase in the crystal size, reaching a maximum and subsequently decreasing. In our case, the dependence of flexural strength on

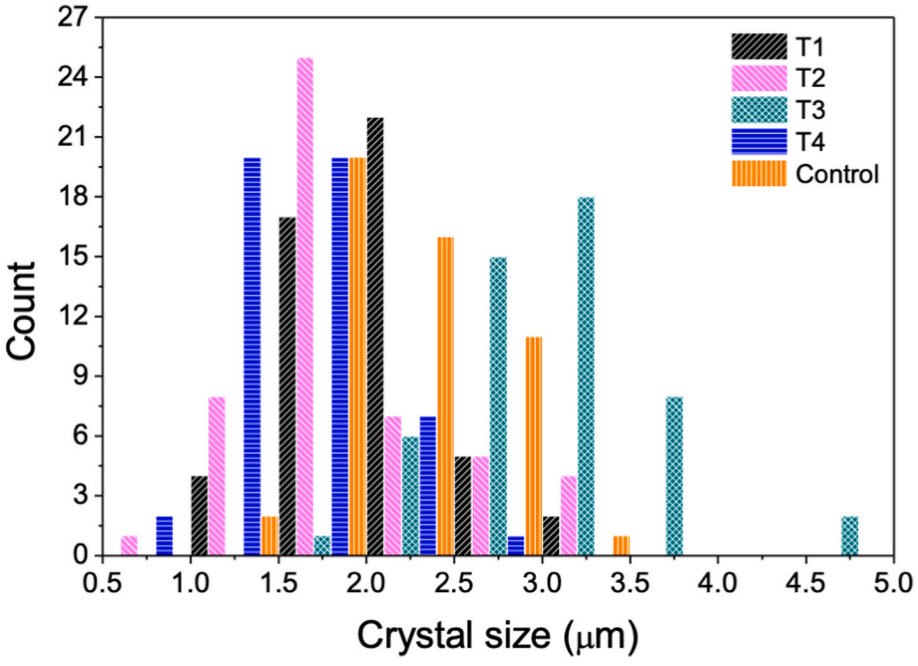

Fig. 3. Crystal size histogram based on each experimental glass-ceramic.

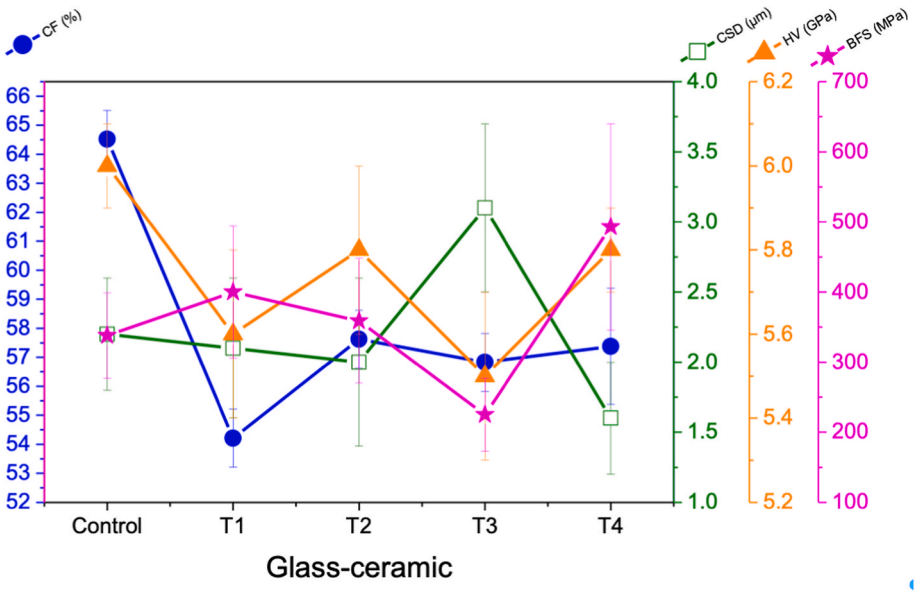

Fig. 4. Crystallized fraction (CF, %), Vickers hardness (HV, GPa), and biaxial flexural strength (BFS, MPa) of each glass-ceramic obtained.

grain size is stronger than on crystallized fraction, since the grain size cannot exceed ~3 μm, as is the case of sample T3, whose crystals reached more than 4 μm (Fig. 3), significantly decreasing the flexural strength.

This feature can be clearly seen in the micrographs in Fig. 1., which show crystals of shorter length and greater number homogeneously dispersed in the vitreous matrix, creating an interlocked network and hindering the propagation of cracks, consequently increasing the values of the analyzed mechanical properties in our study (i.e., elastic modulus, Vickers hardness and flexural strength) [7,25,29,33,71]. It was observed that the BFS values of T1, T2, and T4 were statistically equal to those of the control group (IPS e.max CAD). This can be considered an important feature, as it confirms that the material developed has great potential to be applied as a dental material.

As reported by Serbena et al. [7], the elastic modulus and hardness increase linearly with the crystallized fraction when five reference values (0 %, 10 % 30 % 50 %, and 100 %) of a stoichiometric LS2 are analyzed. In the present study, the elastic modulus was statistically similar for groups T1, T2, and T4, being within the acceptable values in the literature for this type of glass-ceramic [6,18]. In this case, the elastic modulus was probably influenced more by the characteristics of the crystals and their distribution than by the crystallized fraction itself.

The GC obtained herein is in accordance with the description of Serbena et al. [7], with a crystallized fraction above 50 %, which combined with the microstructural characteristics already mentioned with random orientation that results in an intertwining between crystals, is responsible for its high flexural strength.

A strong influence of the crystallized volume fraction [7,72] would be expected. But in this study the crystallized fraction of the different groups (T1-T4) are very close (ranging between 54 and 58 %). Therefore, it can be inferred that based on this there is a strong influence of the morphology and size of the crystal, which must be smaller than 3 μm to achieve hardness and flexural strength values comparable to those of the commercial material. This can be explained based on the study of Serbena et al. [7] the main reasons for its high strength are believed to be its interlocked lath-shaped microstructure and the incompatibility of thermal expansion between the crystal and the glass matrix, which causes residual stresses that can contribute to the crack deflection. and as observed by the authors in the sample with a crystallized volume fraction of 32 %, crack deflection is evident and is associated with the change in the path of the crack when it encounters a crystal.

Thus, this manuscript demonstrates that it is possible to enhance the microstructure and morphology of glass ceramics by varying the temperatures and duration of nucleation, and crystalline growth heat treatments. It results in improvements in the mechanical properties of the experimental materials as observed in groups T2 and T4. Nevertheless, it remains a challenge to create designs that surpass the excellence of materials already available in the dental industry.

5. Conclusions

We developed a lithium silicate glass-ceramic with properties similar to the IPS e.max CAD commercial material. The time and temperature of nucleation heat treatment influenced the size and quantity of crystals and the crystallized fraction, as expected. The elastic modulus agreed with the expected value for lithium silicate glass-ceramics. The best results were found for groups T2 and T4, which were submitted to nucleation temperatures and times of 500 °C/180 min and 480 °C/360 min, respectively. The same crystal growth treatment was used for the formation of LS and LS2 crystalline phases at 700 and 840 °C, respectively. As demonstrated, in addition to the crystallized fraction (which was similar for T2 and T4, that is, ~57 %), there was a strong influence of crystal morphology and size, which must be smaller than 3 μm to reach hardness and flexural strength values comparable to those of the commercial material. In the case of T3, the presence of longer crystals significantly decreased the flexural strength of the material. It was then found that the crystallized fraction and crystal morphology have a significant impact on the mechanical properties and choice of materials in oral rehabilitation, characteristics that are often unknown by dental surgeons. Overall, we could optimize the GC properties through variations in the nucleation time and temperature. Even with a lower crystallized fraction than the control group, we were able to obtain a glass-ceramic with properties comparable to (but not better than) those of a successful commercial material.

Declaration of competing interest

The authors declare that they have no known competing financial interests or personal relationships that could have appeared to influence the work reported in this paper.

Acknowledgements

The authors wish to thank the undergraduate student Arthur T. H.

Olivi from the School of Dentistry at Araraquara, São Paulo State University, for his contribution to this study and the São Paulo Research Foundation (FAPESP) for the financial support (grant number 18/16295-3).

The authors would also like to thank the Coordination for the Improvement of Higher Education Personnel (CAPES) and the São Paulo Research Foundation (FAPESP) through the Center for Research, Technology and Education in Vitreous Materials (CeRTEV) under grant number 2013/07793-6.

We are also grateful to the Laboratory of Advanced Microscopy of the Institute of Chemistry of UNESP, Araraquara, especially Diego Luiz Tita, for the images obtained on the scanning electron microscope, and the post-doctoral student Selma Antonio Gutierrez for analyzing the X-ray diffraction results.

References

[1] J. Deubener, M. Allix, M.J. Davis, A. Duran, T. Höche, T. Honma, T. Komatsu, S. Krüger, I. Mitra, R. Müller, S. Nakane, M.J. Pascual, J.W.P. Schmelzer, E. D. Zanotto, S. Zhou, Updated definition of glass-ceramics, J. Non-Cryst. Solids 501 (2018) 3–10, https://doi.org/10.1016/j.jnoncrysol.2018.01.033.

[2] M. Albakry, M. Guazzato, M.V. Swain, Biaxial flexural strength, elastic moduli, and x-ray diffraction characterization of three pressable all-ceramic materials, J. Prosthet. Dent 89 (2003) 374–380, https://doi.org/10.1067/mpr.2003.42.

[3] L. Alkadi, N.D. Ruse, Fracture toughness of two lithium disilicate dental glass ceramics, J. Prosthet. Dent 116 (2016) 591–596, https://doi.org/10.1016/j.prosdent.2016.02.009.

[4] P.F. Cesar, H.N. Yoshimura, W.G. Miranda, C.L. Miyazaki, L.M. Muta, L.E.R. Filho, Relationship between fracture toughness and flexural strength in dental porcelains, J. Biomed. Mater. Res. 78B (2006) 265–273, https://doi.org/10.1002/jbm.b.30482.

[5] G.F. Ramos, G.K.R. Pereira, M. Amaral, L.F. Valandro, M.A. Bottino, Effect of grinding and heat treatment on the mechanical behavior of zirconia ceramic, Braz. Oral Res. 30 (2016), https://doi.org/10.1590/1807-3107BOR-2016.vol30.0012.

[6] L. Hallmann, P. Ulmer, M. Kern, Effect of microstructure on the mechanical properties of lithium disilicate glass-ceramics, J. Mech. Behav. Biomed. Mater. 82 (2018) 355–370, https://doi.org/10.1016/j.jmbbm.2018.02.032.

[7] F.C. Serbena, I. Mathias, C.E. Foerster, E.D. Zanotto, Crystallization toughening of a model glass-ceramic, Acta Mater. 86 (2015) 216–228, https://doi.org/10.1016/j.actamat.2014.12.007.

[8] M.J. Heffernan, S.A. Aquilino, A.M. Diaz-Arnold, D.R. Haselton, C.M. Stanford, M. A. Vargas, Relative translucency of six all-ceramic systems. Part II: core and veneer materials, J. Prosthet. Dent 88 (2002) 10–15, https://doi.org/10.1067/mpr.2002.126795.

[9] W. Höland, V. Rheinberger, E. Apel, C. van 't Hoen, M. Höland, A. Dommann, M. Obrecht, C. Mauth, U. Graf-Hausner, Clinical applications of glass-ceramics in dentistry, J. Mater. Sci. Mater. Med. 17 (2006) 1037–1042, https://doi.org/10.1007/s10856-006-0441-y.

[10] R.G. Craig, R.L. Sakaguchi, Craig's Restorative Dental Materials, Elsevier, St. Louis, Mo, 2012.

[11] D.G. de França, M.H. Morais, F.D. das Neves, A.F. Carreiro, G.A. Barbosa, Precision fit of screw-retained implant-supported fixed dental prostheses fabricated by CAD/CAM, copy-milling, and conventional methods, Int. J. Oral Maxillofac. Implants 32 (2017) 507–513, https://doi.org/10.11607/jomi.5023.

[12] V. Kassardjian, S. Varma, M. Andiappan, N.H.J. Creugers, D. Bartlett, A systematic review and meta analysis of the longevity of anterior and posterior all-ceramic crowns, J. Dent. 55 (2016) 1–6, https://doi.org/10.1016/j.jdent.2016.08.009.

[13] Y. Zhang, B.R. Lawn, Novel zirconia materials in dentistry, J. Dent. Res. 97 (2018) 140–147, https://doi.org/10.1177/0022034517737483.

[14] F. Zhang, M. Inokoshi, M. Batuk, J. Hadermann, I. Naert, B. Van Meerbeek, J. Vleugels, Strength, toughness and aging stability of highly-translucent Y-TZP ceramics for dental restorations, Dent. Mater. 32 (2016), https://doi.org/10.1016/j.dental.2016.09.025 e327–e337.

[15] S. Pieger, A. Salman, A.S. Bidra, Clinical outcomes of lithium disilicate single crowns and partial fixed dental prostheses: a systematic review, J. Prosthet. Dent 112 (2014) 22–30, https://doi.org/10.1016/j.prosdent.2014.01.005.

[16] F. Zarone, M.I. Di Mauro, P. Ausiello, G. Ruggiero, R. Sorrentino, Current status on lithium disilicate and zirconia: a narrative review, BMC Oral Health 19 (2019) 134, https://doi.org/10.1186/s12903-019-0838-x.

[17] A. Pozzi, L. Arcuri, G. Fabbri, G. Singer, J. Londono, Long-term survival and success of zirconia screw-retained implant-supported prostheses for up to 12 years: a retrospective multicenter study, J. Prosthet. Dent 129 (2023) 96–108, https://doi.org/10.1016/j.prosdent.2021.04.026.

[18] L. Fu, H. Engqvist, W. Xia, Glass-ceramics in dentistry: a review, Materials 13 (2020), https://doi.org/10.3390/ma13051049.

[19] W. Höland, V. Rheinberger, M. Schweiger, Control of nucleation in glass ceramics, philosophical transactions of the royal society of London, Series A: Math. Phys. Eng. Sci. 361 (2003) 575–589, https://doi.org/10.1098/rsta.2002.1152.

[20] T. Zhao, Y. Qin, B. Wang, J.-F. Yang, Improved densification and properties of pressureless-sintered lithium disilicate glass-ceramics, Mater. Sci. Eng., A 620 (2015) 399–406, https://doi.org/10.1016/j.msea.2014.10.037.

[21] P. Zhang, X. Li, J. Yang, S. Xu, Effect of heat treatment on the microstructure and properties of lithium disilicate glass-ceramics, J. Non-Cryst. Solids 402 (2014) 101–105, https://doi.org/10.1016/j.jnoncrysol.2014.05.023.

[22] M. Kamnoy, K. Pengpat, U. Intatha, S. Eitssayeam, Effects of heat treatment temperature on microstructure and mechanical properties of lithium disilicate-based glass-ceramics, Ceram. Int. 44 (2018), https://doi.org/10.1016/j.ceramint.2018.08.223. S121–S124.

[23] H. ÖzdemiR, A. Özdoğan, The effect of heat treatments applied to superstructure porcelain on the mechanical properties and microstructure of lithium disilicate glass ceramics, Dent. Mater. J. 37 (2018) 24–32, https://doi.org/10.4012/dmj.2016-365.

[24] W. Höland, M. Schweiger, R. Watzke, A. Peschke, H. Kappert, Ceramics as biomaterials for dental restoration, Expet Rev. Med. Dev. 5 (2008) 729–745, https://doi.org/10.1586/17434440.5.6.729.

[25] W. Höland, V. Rheinberger, E. Apel, C. van't Hoen, Principles and phenomena of bioengineering with glass-ceramics for dental restoration, J. Eur. Ceram. Soc. 27 (2007) 1521–1526, https://doi.org/10.1016/j.jeurceramsoc.2006.04.101.

[26] J.B. Quinn, V. Sundar, I.K. Lloyd, Influence of microstructure and chemistry on the fracture toughness of dental ceramics, Dent. Mater. 19 (2003) 603–611, https://doi.org/10.1016/S0109-5641(03)00002-2.

[27] H. Riquieri, J.B. Monteiro, D.C. Viegas, T.M.B. Campos, R.M. de Melo, G. de Siqueira Ferreira Anzaloni Saavedra, Impact of crystallization firing process on the microstructure and flexural strength of zirconia-reinforced lithium silicate glass-ceramics, Dent. Mater. 34 (2018) 1483–1491, https://doi.org/10.1016/j.dental.2018.06.010.

[28] F. Wang, J. Gao, H. Wang, J. Chen, Flexural strength and translucent characteristics of lithium disilicate glass–ceramics with different P2O5 content, Mater. Des. 31 (2010) 3270–3274, https://doi.org/10.1016/j.matdes.2010.02.013.

[29] W. Lien, H.W. Roberts, J.A. Platt, K.S. Vandewalle, T.J. Hill, T.-M.G. Chu, Microstructural evolution and physical behavior of a lithium disilicate glass–ceramic, Dent. Mater. 31 (2015) 928–940, https://doi.org/10.1016/j.dental.2015.05.003.

[30] M.O.C. Villas-Boas, F.C. Serbena, V.O. Soares, I. Mathias, E.D. Zanotto, Residual stress effect on the fracture toughness of lithium disilicate glass-ceramics, J. Am. Ceram. Soc. 103 (2020) 465–479, https://doi.org/10.1111/jace.16664.

[31] M. Albakry, M. Guazzato, M.V. Swain, Fracture toughness and hardness evaluation of three pressable all-ceramic dental materials, J. Dent. 31 (2003) 181–188, https://doi.org/10.1016/S0300-5712(03)00025-3.

[32] J. Tinschert, D. Zwez, R. Marx, K.J. Anusavice, Structural reliability of alumina-, feldspar-, leucite-, mica- and zirconia-based ceramics, J. Dent. 28 (2000) 529–535, https://doi.org/10.1016/S0300-5712(00)00030-0.

[33] J.K.M.B. Daguano, M.T.B. Milesi, A.C.D. Rodas, A.F. Weber, J.E.S. Sarkis, M. A. Hortellani, E.D. Zanotto, In vitro biocompatibility of new bioactive lithia-silica glass-ceramics, Mater. Sci. Eng. C 94 (2019) 117–125, https://doi.org/10.1016/j.msec.2018.09.006.

[34] I. Denry, J. Holloway, Ceramics for dental applications: a review, Materials 3 (2010) 351–368, https://doi.org/10.3390/ma3010351.

[35] R. Fabian Fonzar, M. Carrabba, M. Sedda, M. Ferrari, C. Goracci, A. Vichi, Flexural resistance of heat-pressed and CAD-CAM lithium disilicate with different translucencies, Dent. Mater. 33 (2017) 63–70, https://doi.org/10.1016/j.dental.2016.10.005.

[36] S. Huang, B. Zhang, Z. Huang, W. Gao, P. Cao, Crystalline phase formation, microstructure and mechanical properties of a lithium disilicate glass–ceramic, J. Mater. Sci. 48 (2013) 251–257, https://doi.org/10.1007/s10853-012-6738-y.

[37] P.C. Soares, C.M. Lepienski, Residual stress determination on lithium disilicate glass-ceramic by nanoindentation, J. Non-Cryst. Solids 348 (2004) 139–143, https://doi.org/10.1016/j.jnoncrysol.2004.08.139.

[38] X. Zheng, G. Wen, L. Song, X.X. Huang, Effects of P2O5 and heat treatment on crystallization and microstructure in lithium disilicate glass ceramics, Acta Mater. 56 (2008) 549–558, https://doi.org/10.1016/j.actamat.2007.10.024.

[39] G. Wen, X. Zheng, L. Song, Effects of P2O5 and sintering temperature on microstructure and mechanical properties of lithium disilicate glass-ceramics, Acta Mater. 55 (2007) 3583–3591, https://doi.org/10.1016/j.actamat.2007.02.009.

[40] C. Ritzberger, E. Apel, W. Höland, A. Peschke, V. Rheinberger, Properties and clinical application of three types of dental glass-ceramics and ceramics for CAD-CAM technologies, Materials 3 (2010) 3700–3713, https://doi.org/10.3390/ma3063700.

[41] V.O. Soares, F.C. Serbena, I. Mathias, M.C. Crovace, E.D. Zanotto, New, tough and strong lithium metasilicate dental glass-ceramic, Ceram. Int. 47 (2021) 2793–2801, https://doi.org/10.1016/j.ceramint.2020.09.133.

[42] International Standardization Organization, International standard 6872:2008, Dentistry — Ceram. Mater. (2008).

[43] A. Gualtieri, P. Norby, J. Hanson, J. Hriljac, Rietveld refinement using synchrotron X-ray powder diffraction data collected in transmission geometry using an imaging-plate detector: application to standard m -ZrO_2, J. Appl. Crystallogr. 29 (1996) 707–713, https://doi.org/10.1107/S0021889896008199.

[44] B. Bondars, G. Heidemane, J. Grabis, K. Laschke, H. Boysen, J. Schneider, F. Frey, Powder diffraction investigations of plasma sprayed zirconia, J. Mater. Sci. 30 (1995) 1621–1625, https://doi.org/10.1007/BF00375275.

[45] S. Krimm, A.V. Tobolsky, Quantitative x-ray studies of order in amorphous and crystalline polymers. Quantitative x-ray determination of crystallinity in polyethylene, J. Polym. Sci. 7 (1951) 57–76, https://doi.org/10.1002/pol.1951.120070105.

[46] J.K.M.F. Daguano, K. Strecker, E.C. Ziemath, S.O. Rogero, M.H.V. Fernandes, C. Santos, Effect of partial crystallization on the mechanical properties and

cytotoxicity of bioactive glass from the 3CaO.P2O5–SiO2–MgO system, J. Mech. Behav. Biomed. Mater. 14 (2012) 78–88, https://doi.org/10.1016/j.jmbbm.2012.04.024.
[47] T. Ferreira, W. Rasband, ImageJ User Guide: IJ 1.46r Revised Edition, Bethesda, Maryland, USA, 2012.
[48] C.A. Schneider, W.S. Rasband, K.W. Eliceiri, NIH Image to ImageJ: 25 years of image analysis, Nat. Methods 9 (2012) 671–675, https://doi.org/10.1038/nmeth.2089.
[49] ASTM International, ASTM E1876-15, Standard Test Method for Dynamic Young's Modulus, Shear Modulus, and Poisson's Ratio by Impulse Excitation of Vibration, West Conshohocken, PA, 2015. www.astm.org.
[50] L.B. Otani, A.H.A. Pereira, J.D.D. Melo, S.C. Amico, Elastic Moduli Characterization of Composites Using the Impulse Excitation Technique, Ribeirão Preto, São Paulo, Brazil, 2014. Technical-scientific Informative ITC-06/ATCP.
[51] ASTM International, ASTM C1327-03, Standard Test Method for Vickers Indentation Hardness of Advanced Ceramics, West Conshohocken, PA, 2003, https://doi.org/10.1520/C1327-03.
[52] J. Lubauer, K. Hurle, M.R. Cicconi, A. Petschelt, H. Peterlik, U. Lohbauer, R. Belli, Toughening by revitrification of Li2SiO3 crystals in Obsidian® dental glass-ceramic, J. Mech. Behav. Biomed. Mater. 124 (2021), 104739, https://doi.org/10.1016/j.jmbbm.2021.104739.
[53] O. Peitl, E.D. Zanotto, F.C. Serbena, L.L. Hench, Compositional and microstructural design of highly bioactive P2O5–Na2O–CaO, SiO2 glass-Ceram. 8 (2012) 321–332, https://doi.org/10.1016/j.actbio.2011.10.014.
[54] E. Apel, J. Deubener, A. Bernard, M. Höland, R. Müller, H. Kappert, V. Rheinberger, W. Höland, Phenomena and mechanisms of crack propagation in glass-ceramics, J. Mech. Behav. Biomed. Mater. 1 (2008) 313–325, https://doi.org/10.1016/j.jmbbm.2007.11.005.
[55] S. Huang, P. Cao, C. Wang, Z. Huang, W. Gao, Fabrication of a high-strength lithium disilicate glass-ceramic in a complex glass system, J. Asian Ceram. Soc. 1 (2013) 46–52, https://doi.org/10.1016/j.jascer.2013.02.007.
[56] I. Denry, J.A. Holloway, Low temperature sintering of fluorapatite glass-ceramics, Dent. Mater. 30 (2014) 112–121, https://doi.org/10.1016/j.dental.2013.10.009.
[57] C. Duée, F. Désanglois, I. Lebecq, C. Follet-Houttemane, Predicting glass transition and crystallization temperatures of silicate bioglasses using mixture designs, J. Non-Cryst. Solids 358 (2012) 1083–1090, https://doi.org/10.1016/j.jnoncrysol.2012.02.007.
[58] K. Thieme, C. Rüssel, The effect of dopants on crystal growth kinetics of lithium disilicate: surface versus bulk crystallization, J. Mater. Sci. 54 (2019) 1099–1111, https://doi.org/10.1007/s10853-018-2902-3.
[59] D.U. Tulyaganov, S. Agathopoulos, I. Kansal, P. Valério, M.J. Ribeiro, J.M. F. Ferreira, Synthesis and properties of lithium disilicate glass-ceramics in the system SiO2–Al2O3–K2O–Li2O, Ceram. Int. 35 (2009) 3013–3019, https://doi.org/10.1016/j.ceramint.2009.04.002.
[60] H.R. Fernandes, D.U. Tulyaganov, A. Goel, M.J. Ribeiro, M.J. Pascual, J.M. F. Ferreira, Effect of Al2O3 and K2O content on structure, properties and devitrification of glasses in the Li2O–SiO2 system, J. Eur. Ceram. Soc. 30 (2010) 2017–2030, https://doi.org/10.1016/j.jeurceramsoc.2010.04.017.
[61] C.-C. Lin, P. Shen, H.M. Chang, Y.J. Yang, Composition dependent structure and elasticity of lithium silicate glasses: effect of ZrO2 additive and the combination of alkali silicate glasses, J. Eur. Ceram. Soc. 26 (2006) 3613–3620, https://doi.org/10.1016/j.jeurceramsoc.2006.01.010.
[62] J.K.M.B. Daguano, L. Dantas, V.O. Soares, M.F.R.P. Alves, C.D. Santos, E. D. Zanotto, Optimizing the microstructure of a new machinable bioactive glass-ceramic, J. Mech. Behav. Biomed. Mater. 122 (2021), 104695, https://doi.org/10.1016/j.jmbbm.2021.104695.
[63] W. Höland, G.H. Beall, Glass-ceramic Technology, third ed., Wiley-American Ceramic Society, Hoboken, New Jersey, 2019.
[64] S.-H. Kang, J. Chang, H.-H. Son, Flexural strength and microstructure of two lithium disilicate glass ceramics for CAD/CAM restoration in the dental clinic, Restor Dent Endod. 38 (2013) 134, https://doi.org/10.5395/rde.2013.38.3.134.
[65] K. Yuan, F. Wang, J. Gao, X. Sun, Z. Deng, H. Wang, J. Chen, Effect of sintering time on the microstructure, flexural strength and translucency of lithium disilicate glass-ceramics, J. Non-Cryst. Solids 362 (2013) 7–13, https://doi.org/10.1016/j.jnoncrysol.2012.11.010.
[66] S. Huang, P. Cao, Y. Li, Z. Huang, W. Gao, Nucleation and crystallization kinetics of a multicomponent lithium disilicate glass by in situ and real-time synchrotron X-ray diffraction, Cryst. Growth Des. 13 (2013) 4031–4038, https://doi.org/10.1021/cg400835n.
[67] R. Belli, U. Lohbauer, F. Goetz-Neunhoeffer, K. Hurle, Crack-healing during two-stage crystallization of biomedical lithium (di)silicate glass-ceramics, Dent. Mater. 35 (2019) 1130–1145, https://doi.org/10.1016/j.dental.2019.05.013.
[68] V.M. Fokin, R.M.C.V. Reis, A.S. Abyzov, C.R. Chinaglia, J.W.P. Schmelzer, E. D. Zanotto, Non-stoichiometric crystallization of lithium metasilicate–calcium metasilicate glasses. Part 2 — effect of the residual liquid, J. Non-Cryst. Solids 379 (2013) 131–144, https://doi.org/10.1016/j.jnoncrysol.2013.08.006.
[69] R.S. Soares, R.C.C. Monteiro, M.M.R.A. Lima, R.J.C. Silva, Crystallization of lithium disilicate-based multicomponent glasses – effect of silica/lithia ratio, Ceram. Int. 41 (2015) 317–324, https://doi.org/10.1016/j.ceramint.2014.08.074.
[70] J. Lubauer, R. Belli, A. Petschelt, M.R. Cicconi, K. Hurle, U. Lohbauer, Concurrent kinetics of crystallization and toughening in multicomponent biomedical SiO2-Li2O-P2O5-ZrO2 glass-ceramics, J. Non-Cryst. Solids 554 (2021), 120607, https://doi.org/10.1016/j.jnoncrysol.2020.120607.
[71] Z. Zhang, J. Guo, Y. Sun, B. Tian, X. Zheng, M. Zhou, L. He, S. Zhang, Effects of crystal refining on wear behaviors and mechanical properties of lithium disilicate glass-ceramics, J. Mech. Behav. Biomed. Mater. 81 (2018) 52–60, https://doi.org/10.1016/j.jmbbm.2018.02.023.
[72] G.G. Santos, F.C. Serbena, V.M. Fokin, E.D. Zanotto, Microstructure and mechanical properties of nucleant-free Li2O-CaO-SiO2 glass-ceramics, Acta Mater. 130 (2017) 347–360, https://doi.org/10.1016/j.actamat.2017.03.010.